

Electric Toroidal Quadrupoles in Spin-Orbit Coupled Metal $\text{Cd}_2\text{Re}_2\text{O}_7$

Satoru Hayami¹, Yuki Yanagi², Hiroaki Kusunose², and Yukitoshi Motome³

¹*Faculty of Science, Hokkaido University, Sapporo 060-0810, Japan*

²*Department of Physics, Meiji University, Kawasaki 214-8571, Japan*

³*Department of Applied Physics, University of Tokyo, Tokyo 113-8656, Japan*

We report our theoretical results on the order parameters for the pyrochlore metal $\text{Cd}_2\text{Re}_2\text{O}_7$, which undergoes enigmatic phase transitions with inversion symmetry breaking. By carefully examining active electronic degrees of freedom based on the lattice symmetry, we propose that two parity-breaking phases at ambient pressure are described by unconventional multipoles, *electric toroidal quadrupoles* (ETQs) with different components, $x^2 - y^2$ and $3z^2 - r^2$, in the pyrochlore tetrahedral unit. We elucidate that the ETQs are activated by bond or spin-current order on Re-Re bonds. Our ETQ scenario provides a key to reconcile the experimental contradictions, by measuring ETQ specific phenomena, such as peculiar spin splittings in the electronic band structure, magneto-current effect, and nonreciprocal transport under a magnetic field.

Introduction.— The spin-orbit coupling in crystals with the lack of spatial inversion symmetry, dubbed the antisymmetric spin-orbit coupling (ASOC), has attracted great interest in condensed matter physics. It is a source of intriguing phenomena, such as Dirac electrons at the surface of topological insulators [1, 2], the spin Hall effect [3, 4], multiferroics [5–7], and noncentrosymmetric superconductivity [8]. Such ASOC-related physics has been found in a variety of materials irrespective of insulators (semiconductors) [9–12] and metals [13–16] in p -, d -, and f -electron systems. Thus, the ASOC is highly expected to bring a new route toward applications to next-generation electronics and spintronics devices [17, 18].

Of special interest is to control the ASOC by spontaneous inversion symmetry breaking in electronic degrees of freedom. Such parity breaking can generate odd-parity multipoles, e.g., magnetic quadrupoles (MQs) and electric octupoles (EOs) [19–26]. They provide a fertile ground for exploring new types of multipole orders [27–34] and unconventional superconductivities [35–38]. The pyrochlore oxide $\text{Cd}_2\text{Re}_2\text{O}_7$ is a prototype compound for such spontaneous inversion symmetry breaking in the presence of the strong spin-orbit coupling [30, 39]. The system exhibits a surprisingly complex phase diagram while changing temperature and pressure, including a collection of spontaneously parity-breaking phases [40–43]. In addition, among many pyrochlores, it is the only superconductor thus far [44–48]. The superconducting state also shows unconventional behavior under pressure, presumably due to the spontaneous parity breaking [35, 36, 40].

At ambient pressure, $\text{Cd}_2\text{Re}_2\text{O}_7$ undergoes a continuous structural phase transition at $T_{s1} \sim 200$ K, from the centrosymmetric cubic phase with $\text{Fd}\bar{3}\text{m}$ symmetry (phase I) to the noncentrosymmetric tetragonal one (phase II). As the tetragonal lattice distortion is very small, which was evaluated at most 0.05% [49], the transition is considered to be of electronic origin. However, the space-group symmetry in the phase II is still controversial; it was identified as $\text{I}\bar{4}\text{m}2$ by the single-crystal X-ray diffraction (XRD) [49, 50], powder neutron diffraction [51], convergent electron diffraction (CED) [52], Raman spectroscopy [53], nonlinear optics [54],

and polarizing microscope image (PMI) [55], while the recent nonlinear optical measurements indicated further symmetry reduction to $\text{I}\bar{4}$, $\text{I}\bar{4}\text{m}'2'$, or $\text{I}\bar{4}\text{m}'2$ [34, 56, 57]. Moreover, another structural transition to the phase III occurring at $T_{s2} \sim 120$ K is also controversial; the single-crystal XRD [50, 58], CED [52], and PMI [55] measurements indicated a first-order transition to $\text{I}4_122$, while the nonlinear optical measurements indicated the absence of the phase transition [54]. Toward comprehensive understanding of the rich physics by spontaneous parity breaking and emergent ASOC in this compound, it is desired to resolve the experimental contradictions and clarify the origin of the enigmatic phase transitions.

In this Letter, we investigate what types of electronic instability can occur in the spin-orbit coupled metal $\text{Cd}_2\text{Re}_2\text{O}_7$ at ambient pressure from the viewpoint of odd-parity multipoles. Relying on the lattice symmetry by the single-crystal XRD [50], we here concentrate on odd-parity multipoles with E_u symmetry [59]. We find that the order parameters in the phases II and III are described by electric toroidal quadrupoles (ETQs) in the tetrahedral unit of the pyrochlore structure with different components of $x^2 - y^2$ and $3z^2 - r^2$, respectively. We show that spontaneous bond or spin-current ordering on Re-Re bonds is essential to induce the ETQs. We also present how to detect the ETQs in experiments by elucidating ETQ-driven phenomena, such as the spin-split Fermi surface, magneto-current (MC) effect, and nonreciprocal transport (NRT) in an applied magnetic field.

Symmetry argument.— First, we discuss the candidates of order parameters for the phases II and III in $\text{Cd}_2\text{Re}_2\text{O}_7$ from a symmetry point of view. In order to describe the electronic degrees of freedom in crystals, we introduce four types of multipoles: conventional electric (E) and magnetic (M) multipoles (polar and axial tensor, respectively), and unconventional electric toroidal (ET) and magnetic toroidal (MT) multipoles (axial and polar tensor, respectively). They have different parity for spatial inversion (\mathcal{P}) and time-reversal (\mathcal{T}) operations; with respect to $(\mathcal{P}, \mathcal{T})$, E multipole Q_{lm} has the parity $[(-1)^l, +1]$, M multipole M_{lm} has $[(-1)^{l+1}, -1]$, ET multipole G_{lm} has $[(-1)^{l+1}, +1]$, and MT multipole T_{lm} has $[(-1)^l, -1]$, where l and m are the orbital and magnetic quantum numbers, respectively ($-l \leq m \leq l$) [60, 61].

TABLE I. Classification of odd-parity multipoles with respect to the irreducible representation (irrep) of the point group O_h . The superscripts + and - denote time-reversal even and odd, respectively. The odd-parity multipoles are shown with their type, rank, notation, and space group symmetry. ν_{BO} and ν_{SCO} represent the number of modes in each irrep for the bond and spin-current ordered states, respectively.

irrep.	type	rank	notation	symmetry	ν_{BO}	ν_{SCO}
$A_{1u}^+; A_{1u}^-$	ET; M	0	$G_0; M_0$	$F4_132 (O)$	0; 0	1; 1
$A_{2u}^+; A_{2u}^-$	E; MT	3	$Q_{xyz}; T_{xyz}$	$F\bar{4}3m (T_d)$	1; 0	1; 0
$E_u^+; E_u^-$	ET; M	2	$G_u; M_u$	$I4_122 (D_4)$	1; 0	2; 1
			$G_v; M_v$	$I\bar{4}m2 (D_{2d})$		
$T_{1u}^+; T_{1u}^-$	E; MT	1	$Q_z; T_z$	$I4_1 (C_4)$	1; 1	2; 2
			$Q_x; T_x$			
			$Q_y; T_y$			
$T_{2u}^+; T_{2u}^-$	ET; M	2	$G_{xy}; M_{xy}$	$I\bar{4} (S_4)$	0; 1	2; 3
			$G_{yz}; M_{yz}$			
			$G_{zx}; M_{zx}$			

Hence, the types of symmetry breakings are systematically characterized by four types of multipoles with the different rank l . Hereafter, we use the notations for monopole ($l = 0$), dipole ($l = 1$), quadrupole ($l = 2$), and octupole ($l = 3$) as X_0 , (X_x, X_y, X_z) , $(X_u, X_v, X_{yz}, X_{zx}, X_{xy})$, and $(X_{xyz}, X_x^\alpha, X_y^\alpha, X_z^\alpha, X_x^\beta, X_y^\beta, X_z^\beta)$ for E, M, ET, and MT, respectively, where $X = Q, M, G$, and T , and $u = 3z^2 - r^2$ and $v = x^2 - y^2$ [60]. The odd-parity order parameters are characterized by odd-rank E (MT) multipoles and even-rank ET (M) multipoles in the presence (absence) of the time-reversal symmetry.

We classify the odd-parity multipoles in Table I, up to the rank $l = 3$ with respect to the irreducible representation of the cubic O_h group in the phase I. We also present the space subgroup symmetry for each odd-parity multipole within the symmetries supported by the XRD results [50]. Since the XRD measurements [50] indicate that the space group symmetries in the phases II and III are $I\bar{4}m2$ and $I4_122$, respectively, and since $Cd_2Re_2O_7$ is most likely nonmagnetic (time-reversal even) [62], we deduce that the primary order parameters are the ETQs with different components: G_v for the phase II and G_u for the phase III. In the following, we examine what types of electronic instability can induce the two ETQs from a microscopic point of view.

Electric toroidal quadrupoles.— Next, in order to clarify how the ETQs are activated in electronic degrees of freedom, we perform a microscopic analysis based on the tight-binding model. While $Cd_2Re_2O_7$ is a multi-orbital system with relevant t_{2g} orbitals for $5d$ electrons [63–65], we consider an effective single-orbital model and concentrate on the geometrical effect from the pyrochlore structure composed of the tetrahedron unit. An extension to multi-orbital models is straightforward by supplementing additional symmetry operations for atomic orbitals at each site. The Hamiltonian for the effective

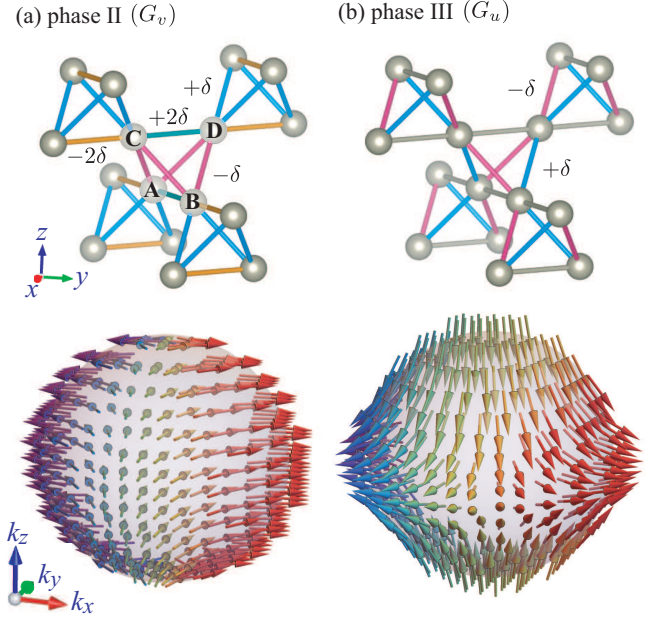


FIG. 1. Schematic pictures of the bond modulations caused by the ETQs: (a) G_u for the phase II and (b) G_v for the phase III. Schematic spin polarizations on one of the Fermi surfaces split by the ETQ orderings are shown in the lower figures.

tight-binding model is given as

$$\mathcal{H} = \sum_{\mathbf{k}\alpha\beta\gamma} \sum_{ij\sigma\sigma'} c_{\mathbf{k}i\sigma}^\dagger [\{f_{\alpha\beta\gamma}^S(\mathbf{k}) + f_{\alpha\beta\gamma}^A(\mathbf{k})\} \rho_{\alpha\tau\beta\sigma\gamma}]_{ij}^{\sigma\sigma'} c_{\mathbf{k}j\sigma'}, \quad (1)$$

where $c_{\mathbf{k}i\sigma}^\dagger$ ($c_{\mathbf{k}i\sigma}$) is the creation (annihilation) operator for wave vector \mathbf{k} , sublattice $i = A-D$, and spin σ . Here, the positions of the four sublattice sites within the tetrahedral unit cell are defined by $\mathbf{r}_A = (0, 0, 0)$, $\mathbf{r}_B = (a/4, a/4, 0)$, $\mathbf{r}_C = (a/4, 0, a/4)$, and $\mathbf{r}_D = (0, a/4, a/4)$ [see Fig. 1(a); we set $a = 1$ as the unit of length]. The four sublattice degree of freedom is described by the product of two Pauli matrices ρ_α and τ_β ; ρ_α spans A-B and C-D, and τ_β spans (AB)-(CD). σ_γ describes 2×2 spin space. $f_{\alpha\beta\gamma}^S(\mathbf{k})$ and $f_{\alpha\beta\gamma}^A(\mathbf{k})$ are symmetric and asymmetric form factors with respect to \mathbf{k} , which are related with even and odd-parity multipoles, respectively. Note that Eq. (1) includes all possibilities of symmetry-breaking mean fields.

As the Hamiltonian in Eq. (1) is an 8×8 matrix denoted by the direct product of three Pauli matrices, $\rho_\alpha\tau_\beta\sigma_\gamma$, the total number of independent electronic degrees of freedom is $8 \times 8 \times 2 = 128$, where the factor 2 comes from symmetric or antisymmetric nature with respect to \mathbf{k} , i.e., $f_{\alpha\beta\gamma}^S$ and $f_{\alpha\beta\gamma}^A$. The 128 electronic degrees of freedom are categorized into the 16 onsite potential types, 96 nearest-neighbor (NN) bond types, and 16 third neighbor bond types. Among them, we neglect the 16 onsite potential-type order parameters, as they do not break spatial inversion symmetry. We also exclude the 16 third-neighbor bond types because their amplitudes are usu-

ally smaller than the NN ones. For the remaining 96 NN bond types, we try to elucidate how they activate the ETQs.

Let us first consider the ETQs without spin degree of freedom. In the spinless subspace, the number of electronic degrees of freedom about the NN bond type is reduced to 24. They are decomposed into the irreducible representations $(A_{1g}^+ \oplus E_g^+ \oplus T_{2g}^+) \oplus (A_{2u}^+ \oplus E_u^+ \oplus T_{1u}^+) \oplus (T_{1g}^- \oplus T_{2g}^-) \oplus (T_{1u}^- \oplus T_{2u}^-)$, where the superscripts + and - represent time-reversal even and odd, respectively. From the decomposition, we find that six types of NN bond modulations can induce odd-parity multipoles of time-reversal even: EO Q_{xyz} , two ETQs (G_u, G_v), and three E dipoles (Q_x, Q_y, Q_z) (see Table I). This indicates that the ETQs G_u and G_v , which we identified as the order parameters in $\text{Cd}_2\text{Re}_2\text{O}_7$, can be activated through spontaneous bond orderings (BO). By taking an appropriate linear combination of $f_{\alpha\beta\gamma}^A(\mathbf{k})\rho_\alpha\tau_\beta\sigma_\gamma$ [66], we obtain the microscopic expressions for the ETQs as

$$\begin{aligned} G_u &= \delta[-s_x c_z \rho_z \tau_y + s_y c_z \rho_y \tau_x + s_z (c_y \rho_x \tau_y - c_x \tau_y)], \\ G_v &= \delta[s_x (2c_y \rho_y \tau_z - c_z \rho_z \tau_y) + s_y (2c_x \rho_y - c_z \rho_y \tau_x) \\ &\quad - s_z (c_x \tau_y + c_y \rho_x \tau_y)], \end{aligned} \quad (2) \quad (3)$$

where $s_\mu = \sin(k_\mu/4)$ and $c_\mu = \cos(k_\mu/4)$ ($\mu = x, y, z$), and δ represents the degree of bond distortions, which corresponds to the order parameter amplitude. The bond modulations are schematically shown in Fig. 1: (a) for G_v in the phase II [Eq. (3)] and (b) for G_u in the phase III [Eq. (2)]. Note that each atomic site is no longer the inversion center in these states, reflecting the odd parity of G_u and G_v . We list the number of modes (independent order parameters) in the BO states in Table I.

We next discuss the ETQs with spin degree of freedom. As spins are time-reversal odd, the odd-parity multipoles of time-reversal even are constructed by combining the Pauli matrix σ_γ and the above spinless odd-parity multipoles with time-reversal odd, i.e., the MT dipoles (MTD) (T_x, T_y, T_z) belonging to T_{1u}^- and MQs (M_{yz}, M_{zx}, M_{xy}) belonging to T_{2u}^- , as shown in Table I. By regarding σ_γ as an axial M dipole belonging to T_{2g}^- , the odd-parity multipoles of time-reversal even in the spinful case are obtained in the irreducible representations of $(T_{1u}^- \oplus T_{2u}^-) \otimes T_{2g}^- \rightarrow A_{1u}^+ \oplus A_{2u}^+ \oplus 2E_u^+ \oplus 2T_{1u}^+ \oplus 2T_{2u}^+$. Consequently, we find four types of active ETQs, $2E_u^+$, whose microscopic expressions are represented by

$$G_u^{\sigma(1)} = 2\sigma_z T_z - \sigma_x T_x - \sigma_y T_y, \quad (4)$$

$$G_u^{\sigma(2)} = \sigma_x M_{yz} - \sigma_y M_{zx}, \quad (5)$$

$$G_v^{\sigma(1)} = \sigma_x T_x - \sigma_y T_y, \quad (6)$$

$$G_v^{\sigma(2)} = 2\sigma_z M_{xy} - \sigma_x M_{yz} - \sigma_y M_{zx}, \quad (7)$$

where the superscript σ denotes that the ETQs have spin dependence; (T_x, T_y, T_z) and (M_{yz}, M_{zx}, M_{xy}) are given

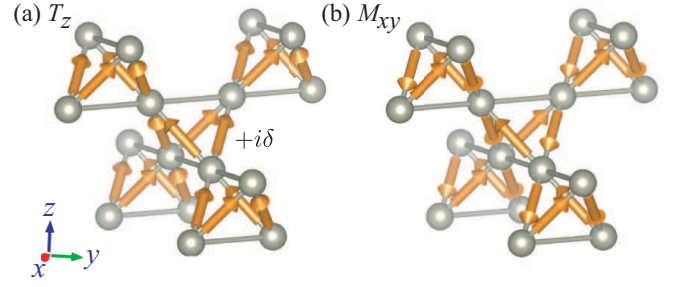


FIG. 2. Schematic pictures of the bond modulations in the presence of (a) the MTD T_z in Eq. (10) and (b) the MQ M_{xy} in Eq. (13). The arrows on the bonds represent the imaginary hoppings.

as [66]

$$T_x = \delta[s_x (c_y \rho_x + c_z \tau_x) + s_y c_x \rho_x \tau_z + s_z c_x \rho_z \tau_x], \quad (8)$$

$$T_y = \delta[s_x c_y \rho_x \tau_z + s_y (c_x \rho_x + c_z \rho_x \tau_x) - s_z c_y \rho_y \tau_y], \quad (9)$$

$$T_z = \delta[s_x c_z \rho_z \tau_x - s_y c_z \rho_y \tau_y + s_z (c_x \tau_x + c_y \rho_x \tau_x)], \quad (10)$$

$$M_{yz} = \delta[s_x (c_z \tau_x - c_y \rho_x) - s_y c_x \rho_x \tau_z + s_z c_x \rho_z \tau_x], \quad (11)$$

$$M_{zx} = \delta[s_x c_y \rho_x \tau_z + s_y (c_x \rho_x - c_z \rho_x \tau_x) + s_z c_y \rho_y \tau_y], \quad (12)$$

$$M_{xy} = -\delta[s_x c_z \rho_z \tau_x + s_y c_z \rho_y \tau_y - s_z (c_y \rho_x \tau_x - c_x \tau_x)]. \quad (13)$$

The ETQs in Eqs. (4)-(7) are also activated through a bond-order type instability as those in the spinless case in Eqs. (2) and (3). However, they originate from asymmetric modulations of time-reversal-odd imaginary hoppings in the spin-dependent form, which can be regarded as spin-current orders (SCOs). In Fig. 2, we exemplify the MTD T_z [Eq. (10)] and MQ M_{xy} [Eq. (13)], in which the arrows on each bond represent the imaginary hoppings [67]. This type of SCO has been studied in the context of spontaneous topological Mott insulators [68, 69]. We list the number of modes in the SCO state in Table I.

Secondary order parameters.— As direct observation of ETQs is rather difficult, we discuss what types of multipoles are additionally induced as the secondary order parameters under the ETQ orders from symmetry arguments [61]. In the phase II with $I4m2$ (D_{2d}) symmetry, since A_{2u} reduces to symmetric representations A_1 , the odd-parity EO Q_{xyz} is induced as a secondary order parameter. Meanwhile, in the phase III, the odd-parity ET monopole (ETM) G_0 (time-reversal even pseudoscalar) is induced as a secondary order parameter, since A_{1u} reduces to symmetric representations under the $I4_122$ (D_4) symmetry. Furthermore, in both phases II and III, since E_g reduces to symmetric representations $A_1 \oplus B_1$, the even-parity E quadrupole (EQ) Q_u is induced as a secondary order parameter. The observation of these secondary order parameters can be indirect evidences of the ETQ orders. For instance, ultrasound and magnetic torque measurements may detect the EQ.

ETQ-driven phenomena.— For further identification of the ETQs, we discuss physical phenomena driven by the ETQ orderings. As the ETQs break spatial inversion symmetry, the

TABLE II. Nonzero components of the MC tensor α_{ij} and NRT tensor σ_{ijkl} expected under the ETQ orderings. The results for the NRT are shown for both primary (op1) and secondary (op2) order parameters. See the text for details.

Phase II op1: G_v (ETQ), op2: Q_{xyz} (EO), Q_u (EQ)	
MC	$\alpha_{xx} = -\alpha_{yy}$
NRT	$\sigma_{xxxx} = -\sigma_{yyyy}, \sigma_{xxyy} = -\sigma_{yyxx}, \sigma_{xyyx} = -\sigma_{yxxy},$ $\sigma_{xxzz} = -\sigma_{yyzz}, \sigma_{zzxx} = -\sigma_{zzyy}, \sigma_{zzzz} = -\sigma_{zzyy},$ $\sigma_{zzzz} = -\sigma_{zzyy}$
Phase III op1: G_u (ETQ), op2: G_0 (ETM), Q_u (EQ)	
MC	$\alpha_{xx} = \alpha_{yy}, \alpha_{zz}$
NRT	$\sigma_{xxxx} = \sigma_{yyyy}, \sigma_{xxyy} = \sigma_{yyxx}, \sigma_{xyyx} = \sigma_{yxxy},$ $\sigma_{xxzz} = \sigma_{yyzz}, \sigma_{zzxx} = \sigma_{zzyy}, \sigma_{zzzz} = \sigma_{zzyy},$ $\sigma_{zzzz} = \sigma_{zzyy}, \sigma_{zzzz}$

band structures in both phases II and III exhibit spin splitting as the Rashba metals [30, 56]. The origin of such spin splitting is the ASOC induced by the ETQ orderings. The functional form of the ASOC is derived by considering the active odd-parity multipoles belonging to symmetric representations in their space groups [61, 70]; namely, G_v and Q_{xyz} in the phase II, and G_u and G_0 in the phase III. In particular, the odd-parity multipoles with rank 0-2 lead to the ASOC in the first order of k [61]. The resultant functional forms of the ASOC for the phases II and III are given by

$$\mathcal{H}_{\text{ASOC}}^{\text{II}} = c_1(k_x\sigma_x - k_y\sigma_y) + \mathcal{O}(k^3), \quad (14)$$

$$\mathcal{H}_{\text{ASOC}}^{\text{III}} = c_1(k_x\sigma_x + k_y\sigma_y) + c_2k_z\sigma_z + \mathcal{O}(k^3), \quad (15)$$

respectively, where c_1 and c_2 are appropriate constants proportional to the order parameter amplitude δ . The spin polarizations on the spin-split Fermi surface are schematically shown for the phases II and III in the lower pictures of Figs. 1(a) and 1(b), respectively. Note that such spin splitting in the band structure occurs even for the spinless ETQs in Eqs. (2) and (3) in the presence of the spin-orbit coupling.

In addition, the ETQs give rise to intriguing responses to external stimuli. One is the MC effect, in which a uniform magnetization M_i is induced by an electric current J_j ($i, j = x, y, z$) as [61, 70]

$$M_i = \alpha_{ij}J_j, \quad (16)$$

where the MC tensor α_{ij} is the rank-2 axial tensor of time-reversal even. The form of α_{ij} is related with active odd-parity multipoles with rank 0-2 ($G_0 \oplus Q_{1m} \oplus G_{2m}$) [61]; the rank-0, 1, and 2 multipoles have the isotropic, antisymmetric, and symmetric traceless components, respectively. Thus, α_{ij} in the phase II becomes symmetric and traceless corresponding to G_v : $\alpha_{xx} = -\alpha_{yy} \propto G_v$. Meanwhile, α_{ij} in the phase III has two nonzero symmetric components reflecting G_0 and G_u : $\alpha_{xx} = \alpha_{yy} \propto G_0 - G_u$ and $\alpha_{zz} \propto G_0 + 2G_u$. The results are summarized in Table II.

Another interesting response is the NRT. As a nonreciprocal current is proportional to the second order of an electric field,

the NRT needs the breaking of time-reversal symmetry by an external magnetic field as

$$J_i = \sigma_{ijkl}E_jE_kH_l, \quad (17)$$

where the NRT tensor σ_{ijkl} is the rank-4 axial tensor; E_j and H_l are electric and magnetic fields, respectively. From symmetry arguments, the form of the NRT tensor is related with the multipoles with rank 0-4 ($2G_0 \oplus 3Q_{1m} \oplus 4G_{2m} \oplus 2Q_{3m} \oplus G_{4m}$) [61]. Consequently, σ_{ijkl} has independent seven (eight) components in the phase II (III), as shown in Table II. We note that higher-order ET hexadecapoles also become active: G_{4v} in the phase II, and G_4 and G_{4u} in the phase III.

It is also interesting to point out that a lattice distortion is induced by an electric current in an applied magnetic field as $\zeta_{ij} = d_{ijkl}J_kH_l$ where d_{ijkl} represents a strain tensor [61, 70]. This is easily understood by noting that E_jE_k in Eq. (17) and ζ_{ij} show the same transformation under the space-time inversion. Thus, the tensor d_{ijkl} has similar nonzero components as σ_{ijkl} in Eq. (17).

Conclusion.— We theoretically showed that the odd-parity ETQs with different components of $x^2 - y^2$ and $3z^2 - r^2$ are the candidates of the primary order parameters in the phases II and III, respectively, in the spin-orbit coupled metal $\text{Cd}_2\text{Re}_2\text{O}_7$. We clarified that electronic instabilities toward spontaneous bond or spin-current ordering on Re-Re bonds induce the ETQ orders. We also discussed how to identify the ETQs by exemplifying their characteristic phenomena, such as spin-split Fermi surfaces, MC effect, and NRT in an applied magnetic field. Our ETQ scenario will give an insight into the origin of the enigmatic phase transitions in $\text{Cd}_2\text{Re}_2\text{O}_7$. Furthermore, our microscopic classifications of multipoles are widely applicable to other spontaneously parity-breaking systems.

The authors thank Z. Hiroi, J. Yamaura, S. Uji, D. Hirai, and H. Hirose for the fruitful discussions on experimental information in $\text{Cd}_2\text{Re}_2\text{O}_7$. This research was supported by JSPS KAKENHI Grants Numbers JP15H05885, JP18H04296 (J-Physics), and JP18K13488.

-
- [1] M. Z. Hasan and C. L. Kane, Rev. Mod. Phys. **82**, 3045 (2010).
 - [2] X.-L. Qi and S.-C. Zhang, Rev. Mod. Phys. **83**, 1057 (2011).
 - [3] J. E. Hirsch, Phys. Rev. Lett. **83**, 1834 (1999).
 - [4] J. Sinova, D. Culcer, Q. Niu, N. A. Sinitsyn, T. Jungwirth, and A. H. MacDonald, Phys. Rev. Lett. **92**, 126603 (2004).
 - [5] M. Fiebig, J. Phys. D: Appl. Phys. **38**, R123 (2005).
 - [6] S.-W. Cheong and M. Mostovoy, Nat. Mater. **6**, 13 (2007).
 - [7] D. Khomskii, Physics **2**, 20 (2009).
 - [8] E. Bauer and M. Sigrist, eds., Non-Centrosymmetric Superconductors: Introduction and Overview (Lecture Notes in Physics) (Springer, 2012), 2012th ed., ISBN 9783642246234.
 - [9] M. S. Dresselhaus, G. Dresselhaus, and A. Jorio, Group Theory: Application to the Physics of Condensed Matter (Springer-Verlag, Berlin Heidelberg, 2008).

- [10] K. Ishizaka, M. Bahramy, H. Murakawa, M. Sakano, T. Shimojima, T. Sonobe, K. Koizumi, S. Shin, H. Miyahara, A. Kimura, et al., *Nat. mater.* **10**, 521 (2011).
- [11] T. Furukawa, Y. Shimokawa, K. Kobayashi, and T. Itou, *Nat. Commun.* **8**, 954 (2017).
- [12] T. Ideue, K. Hamamoto, S. Koshikawa, M. Ezawa, S. Shimizu, Y. Kaneko, Y. Tokura, N. Nagaosa, and Y. Iwasa, *Nat. Phys.* **13**, 578 (2017).
- [13] E. Bauer, G. Hilscher, H. Michor, C. Paul, E. W. Scheidt, A. Griбанov, Y. Seropegin, H. Noël, M. Sigrist, and P. Rogl, *Phys. Rev. Lett.* **92**, 027003 (2004).
- [14] A. Ashrafi and D. L. Maslov, *Phys. Rev. Lett.* **109**, 227201 (2012).
- [15] W. Witczak-Krempa, G. Chen, Y. B. Kim, and L. Balents, *Annu. Rev. Condens. Matter Phys.* **5**, 57 (2014).
- [16] H. Saito, K. Uenishi, N. Miura, C. Tabata, H. Hidaka, T. Yanagisawa, and H. Amitsuka, *J. Phys. Soc. Jpn.* **87**, 033702 (2018).
- [17] I. Žutić, J. Fabian, and S. Das Sarma, *Rev. Mod. Phys.* **76**, 323 (2004).
- [18] V. Baltz, A. Manchon, M. Tsoi, T. Moriyama, T. Ono, and Y. Tserkovnyak, *Rev. Mod. Phys.* **90**, 015005 (2018).
- [19] Y. Yanase, *J. Phys. Soc. Jpn.* **83**, 014703 (2014).
- [20] T. Hitomi and Y. Yanase, *J. Phys. Soc. Jpn.* **83**, 114704 (2014).
- [21] T. Hitomi and Y. Yanase, *J. Phys. Soc. Jpn.* **85**, 124702 (2016).
- [22] K. Kimura, P. Babkevich, M. Sera, M. Toyoda, K. Yamauchi, G. Tucker, J. Martius, T. Fennell, P. Manuel, D. Khalyavin, et al., *Nat. Commun.* **7**, 13039 (2016).
- [23] Y. Kato, K. Kimura, A. Miyake, M. Tokunaga, A. Matsuo, K. Kindo, M. Akaki, M. Hagiwara, M. Sera, T. Kimura, et al., *Phys. Rev. Lett.* **118**, 107601 (2017).
- [24] N. D. Khanh, N. Abe, S. Kimura, Y. Tokunaga, and T. Arima, *Phys. Rev. B* **96**, 094434 (2017).
- [25] Y. Yanagi, S. Hayami, and H. Kusunose, *Phys. Rev. B* **97**, 020404 (2018).
- [26] S. Hayami, H. Kusunose, and Y. Motome, *Phys. Rev. B* **97**, 024414 (2018).
- [27] E. Fradkin, S. A. Kivelson, M. J. Lawler, J. P. Eisenstein, and A. P. Mackenzie, *Annu. Rev. Condens. Matter Phys.* **1**, 153 (2010).
- [28] S. Hayami, H. Kusunose, and Y. Motome, *Phys. Rev. B* **90**, 024432 (2014).
- [29] S. Hayami, H. Kusunose, and Y. Motome, *Phys. Rev. B* **90**, 081115 (2014).
- [30] L. Fu, *Phys. Rev. Lett.* **115**, 026401 (2015).
- [31] M. R. Norman, *Phys. Rev. B* **92**, 075113 (2015).
- [32] S. Hayami, H. Kusunose, and Y. Motome, *J. Phys.: Condens. Matter* **28**, 395601 (2016).
- [33] H. Watanabe and Y. Yanase, *Phys. Rev. B* **96**, 064432 (2017).
- [34] S. Di Matteo and M. R. Norman, *Phys. Rev. B* **96**, 115156 (2017).
- [35] V. Kozii and L. Fu, *Phys. Rev. Lett.* **115**, 207002 (2015).
- [36] Y. Wang, G. Y. Cho, T. L. Hughes, and E. Fradkin, *Phys. Rev. B* **93**, 134512 (2016).
- [37] F. Wu and I. Martin, *Phys. Rev. B* **96**, 144504 (2017).
- [38] S. Sumita, T. Nomoto, and Y. Yanase, *Phys. Rev. Lett.* **119**, 027001 (2017).
- [39] Z. Hiroi, J.-i. Yamaura, T. C. Kobayashi, Y. Matsubayashi, and D. Hirai, *J. Phys. Soc. Jpn.* **87**, 024702 (2017).
- [40] T. C. Kobayashi, Y. Irie, J.-i. Yamaura, Z. Hiroi, and K. Murata, *J. Phys. Soc. Jpn.* **80**, 023715 (2011).
- [41] N. Barišić, L. Forró, D. Mandrus, R. Jin, J. He, and P. Fazekas, *Phys. Rev. B* **67**, 245112 (2003).
- [42] J.-i. Yamaura, K. Takeda, Y. Ikeda, N. Hirao, Y. Ohishi, T. C. Kobayashi, and Z. Hiroi, *Phys. Rev. B* **95**, 020102 (2017).
- [43] I. A. Sergienko and S. H. Curnoe, *J. Phys. Soc. Jpn.* **72**, 1607 (2003).
- [44] M. Hanawa, Y. Muraoka, T. Tayama, T. Sakakibara, J. Yamaura, and Z. Hiroi, *Phys. Rev. Lett.* **87**, 187001 (2001).
- [45] H. Sakai, K. Yoshimura, H. Ohno, H. Kato, S. Kambe, R. E. Walstedt, T. D. Matsuda, Y. Haga, and Y. Onuki, *J. Phys.: Condens. Matter* **13**, L785 (2001).
- [46] R. Jin, J. He, S. McCall, C. S. Alexander, F. Drymiotis, and D. Mandrus, *Phys. Rev. B* **64**, 180503 (2001).
- [47] Z. Hiroi, T. Yamauchi, T. Yamada, M. Hanawa, Y. Ohishi, O. Shimomura, M. Abliz, M. Hedo, and Y. Uwatoko, *J. Phys. Soc. Jpn.* **71**, 1553 (2002).
- [48] Z. Hiroi and M. Hanawa, *J. Phys. Chem. Solids* **63**, 1021 (2002).
- [49] J. P. Castellan, B. D. Gaulin, J. van Duijn, M. J. Lewis, M. D. Lumsden, R. Jin, J. He, S. E. Nagler, and D. Mandrus, *Phys. Rev. B* **66**, 134528 (2002).
- [50] J.-I. Yamaura and Z. Hiroi, *J. Phys. Soc. Jpn.* **71**, 2598 (2002).
- [51] M. T. Weller, R. W. Hughes, J. Rooke, C. S. Knee, and J. Reading, *Dalton Trans.* pp. 3032–3041 (2004).
- [52] K. Tsuda, M. Oishi, M. Tanaka, M. Hanawa, and Z. Hiroi, *Abstracts of the Physical Society of Japan (Annual Meeting, March, 2002 Part 3*, 562 (2002).
- [53] C. A. Kendziora, I. A. Sergienko, R. Jin, J. He, V. Keppens, B. C. Sales, and D. Mandrus, *Phys. Rev. Lett.* **95**, 125503 (2005).
- [54] J. C. Petersen, M. D. Caswell, J. S. Dodge, I. A. Sergienko, J. He, R. Jin, and D. Mandrus, *Nature Physics* **2**, 605 (2006).
- [55] Y. Matsubayashi, D. Hirai, M. Tokunaga, and Z. Hiroi, *J. Phys. Soc. Jpn.* **87**, 104604 (2018).
- [56] J. Harter, Z. Zhao, J.-Q. Yan, D. Mandrus, and D. Hsieh, *Science* **356**, 295 (2017).
- [57] J. W. Harter, D. M. Kennes, H. Chu, A. de la Torre, Z. Y. Zhao, J.-Q. Yan, D. G. Mandrus, A. J. Millis, and D. Hsieh, *Phys. Rev. Lett.* **120**, 047601 (2018).
- [58] F. Razavi, Y. Rohanizadegan, M. Hajialamdari, M. Reedyk, R. Kremer, and B. Mitrović, *Can. J. Phys.* **93**, 1646 (2015).
- [59] Note1, the analysis is straightforwardly applicable to another symmetry like T_{2u} suggested in Refs. [56, 57].
- [60] S. Hayami and H. Kusunose, *J. Phys. Soc. Jpn.* **87**, 033709 (2018).
- [61] S. Hayami, M. Yatsushiro, Y. Yanagi, and H. Kusunose, *Phys. Rev. B* **98**, 165110 (2018).
- [62] O. Vyaselev, K. Arai, K. Kobayashi, J. Yamazaki, K. Kodama, M. Takigawa, M. Hanawa, and Z. Hiroi, *Phys. Rev. Lett.* **89**, 017001 (2002).
- [63] D. J. Singh, P. Blaha, K. Schwarz, and J. O. Sofo, *Phys. Rev. B* **65**, 155109 (2002).
- [64] H. Harima, *J. Phys. Chem. Solids* **63**, 1035 (2002).
- [65] Y. Yanagi, in preparation.
- [66] See Supplemental Materials at (xx) for microscopic expressions of ETQs in Eqs. (2), (3), (8)-(13).
- [67] Note2, note that the imaginary hoppings correspond to the MTD on the bond centers. In fact, the BO state in Fig. 2(a) has a net MT dipole moment.
- [68] S. Raghu, X.-L. Qi, C. Honerkamp, and S.-C. Zhang, *Phys. Rev. Lett.* **100**, 156401 (2008).
- [69] M. Kurita, Y. Yamaji, and M. Imada, *J. Phys. Soc. Jpn.* **80**, 044708 (2011).
- [70] H. Watanabe and Y. Yanase, arXiv:1805.10828 (2018).

Supplemental material for
“Electric Toroidal Quadrupoles in Spin-Orbit Coupled Metal Cd₂Re₂O₇”

Microscopic expressions of electric toroidal quadrupoles

We present a derivation of the microscopic expressions of ETQs in Eqs. (2), (3), (8)-(13) in the main text. First, we consider multiple degrees of freedom on a unit of tetrahedron. The irreducible representation of molecular orbitals under the T_d group is given by $A_1 \oplus T_2$. Then, the basis wave functions are expressed as

$$A_1 : \psi_{A_1} = \frac{1}{2}(\psi_A + \psi_B + \psi_C + \psi_D), \quad (18)$$

$$T_2 : \psi_{T_{2,x}} = \frac{1}{2}(-\psi_A + \psi_B + \psi_C - \psi_D), \quad (19)$$

$$\psi_{T_{2,y}} = \frac{1}{2}(-\psi_A + \psi_B - \psi_C + \psi_D), \quad (20)$$

$$\psi_{T_{2,z}} = \frac{1}{2}(-\psi_A - \psi_B + \psi_C + \psi_D), \quad (21)$$

where ψ_i is the s -wave-like atomic wave function at site $i = A-D$ [see Fig. 1(a) in the main text]. For these basis functions, there are sixteen electronic degrees of freedom, which are decomposed by the irreducible representation of the symmetry of a unit of tetrahedron, T_d , as

$$(A_1 \oplus T_2) \otimes (A_1 \oplus T_2) = (2A_1^+ \oplus E^+ \oplus 2T_2^+) \oplus (T_1^- \oplus T_2^-). \quad (22)$$

As the molecular orbitals ψ_{A_1} and $\psi_{T_2} = (\psi_{T_{2,x}}, \psi_{T_{2,y}}, \psi_{T_{2,z}})$ have the same symmetry properties as the atomic orbitals s and (p_x, p_y, p_z) , respectively, these electronic degrees of freedom are represented by sixteen independent multipoles in an s - p hybridized system [60]: two electric monopoles $\tilde{Q}_0^{(1)}$ and $\tilde{Q}_0^{(2)}$ belonging to A_1^+ , two electric quadrupoles (\tilde{Q}_u, \tilde{Q}_v) belonging to E^+ , three electric dipoles ($\tilde{Q}_x, \tilde{Q}_y, \tilde{Q}_z$) and other three electric quadrupoles ($\tilde{Q}_{yz}^{(1)}, \tilde{Q}_{zx}^{(1)}, \tilde{Q}_{xy}^{(1)}$) belonging to T_2^+ , three magnetic dipoles ($\tilde{M}_x, \tilde{M}_y, \tilde{M}_z$) belonging to T_1^- , and three magnetic toroidal dipoles ($\tilde{T}_x, \tilde{T}_y, \tilde{T}_z$) belonging to T_2^- . The matrix elements for each multipole in the basis functions ($\psi_{A_1}, \psi_{T_{2,x}}, \psi_{T_{2,y}}, \psi_{T_{2,z}}$) are given by [60]

$$\tilde{Q}_0^{(1)} = \begin{pmatrix} 1 & 0 & 0 & 0 \\ 0 & 1 & 0 & 0 \\ 0 & 0 & 1 & 0 \\ 0 & 0 & 0 & 1 \end{pmatrix}, \quad \tilde{Q}_0^{(2)} = \begin{pmatrix} 3 & 0 & 0 & 0 \\ 0 & -1 & 0 & 0 \\ 0 & 0 & -1 & 0 \\ 0 & 0 & 0 & -1 \end{pmatrix}, \quad (23)$$

$$\tilde{Q}_x = \begin{pmatrix} 0 & -2 & 0 & 0 \\ -2 & 0 & 0 & 0 \\ 0 & 0 & 0 & 0 \\ 0 & 0 & 0 & 0 \end{pmatrix}, \quad \tilde{Q}_y = \begin{pmatrix} 0 & 0 & -2 & 0 \\ 0 & 0 & 0 & 0 \\ -2 & 0 & 0 & 0 \\ 0 & 0 & 0 & 0 \end{pmatrix}, \quad \tilde{Q}_z = \begin{pmatrix} 0 & 0 & 0 & -2 \\ 0 & 0 & 0 & 0 \\ 0 & 0 & 0 & 0 \\ -2 & 0 & 0 & 0 \end{pmatrix}, \quad (24)$$

$$\tilde{Q}_u = \begin{pmatrix} 0 & 0 & 0 & 0 \\ 0 & 2 & 0 & 0 \\ 0 & 0 & 2 & 0 \\ 0 & 0 & 0 & -4 \end{pmatrix}, \quad \tilde{Q}_v = \begin{pmatrix} 0 & 0 & 0 & 0 \\ 0 & -2 & 0 & 0 \\ 0 & 0 & 2 & 0 \\ 0 & 0 & 0 & 0 \end{pmatrix}, \quad (25)$$

$$\tilde{Q}_{yz}^{(1)} = \begin{pmatrix} 0 & 0 & 0 & 0 \\ 0 & 0 & 0 & 0 \\ 0 & 0 & 0 & 2 \\ 0 & 0 & 2 & 0 \end{pmatrix}, \quad \tilde{Q}_{zx}^{(1)} = \begin{pmatrix} 0 & 0 & 0 & 0 \\ 0 & 0 & 0 & 2 \\ 0 & 0 & 0 & 0 \\ 0 & 2 & 0 & 0 \end{pmatrix}, \quad \tilde{Q}_{xy}^{(1)} = \begin{pmatrix} 0 & 0 & 0 & 0 \\ 0 & 0 & 2 & 0 \\ 0 & 2 & 0 & 0 \\ 0 & 0 & 0 & 0 \end{pmatrix}, \quad (26)$$

$$\tilde{M}_x = \begin{pmatrix} 0 & 0 & 0 & 0 \\ 0 & 0 & 0 & 0 \\ 0 & 0 & 0 & -2i \\ 0 & 0 & 2i & 0 \end{pmatrix}, \quad \tilde{M}_y = \begin{pmatrix} 0 & 0 & 0 & 0 \\ 0 & 0 & 0 & 2i \\ 0 & 0 & 0 & 0 \\ 0 & -2i & 0 & 0 \end{pmatrix}, \quad \tilde{M}_z = \begin{pmatrix} 0 & 0 & 0 & 0 \\ 0 & 0 & -2i & 0 \\ 0 & 2i & 0 & 0 \\ 0 & 0 & 0 & 0 \end{pmatrix}, \quad (27)$$

$$\tilde{T}_x = \begin{pmatrix} 0 & -2i & 0 & 0 \\ 2i & 0 & 0 & 0 \\ 0 & 0 & 0 & 0 \\ 0 & 0 & 0 & 0 \end{pmatrix}, \quad \tilde{T}_y = \begin{pmatrix} 0 & 0 & -2i & 0 \\ 0 & 0 & 0 & 0 \\ 2i & 0 & 0 & 0 \\ 0 & 0 & 0 & 0 \end{pmatrix}, \quad \tilde{T}_z = \begin{pmatrix} 0 & 0 & 0 & -2i \\ 0 & 0 & 0 & 0 \\ 0 & 0 & 0 & 0 \\ 2i & 0 & 0 & 0 \end{pmatrix}, \quad (28)$$

where we take appropriate normalizations to simplify the following expressions. Note that $(\tilde{Q}_x, \tilde{Q}_y, \tilde{Q}_z)$ in Eq. (24) and $(\tilde{T}_x, \tilde{T}_y, \tilde{T}_z)$ in Eq. (28) are the odd-parity multipoles. In the following calculations for the centrosymmetric pyrochlore structure (point group O_h) consisting of upward and downward tetrahedra, these odd-parity multipoles are replaced by the even-parity multipoles in the same irreducible representation as $(\tilde{Q}_x, \tilde{Q}_y, \tilde{Q}_z) \rightarrow (\tilde{Q}_{yz}^{(2)}, \tilde{Q}_{zx}^{(2)}, \tilde{Q}_{xy}^{(2)})$ and $(\tilde{T}_x, \tilde{T}_y, \tilde{T}_z) \rightarrow (\tilde{T}_{yz}, \tilde{T}_{zx}, \tilde{T}_{xy})$. By a unitary transformation, the multipole degrees of freedom for a unit of tetrahedron in the pyrochlore structure in the basis $(\psi_A, \psi_B, \psi_C, \psi_D)$ can be expressed as

$$A_{1g}^+ : Q_0^{(1)} = 1, Q_0^{(2)} = \rho_x + \tau_x + \rho_x \tau_x, \quad (29)$$

$$E_g^+ : (Q_u, Q_v) = (\tau_x - 2\rho_x + \rho_x \tau_x, \tau_x - \rho_x \tau_x), \quad (30)$$

$$T_{2g}^+ : (Q_{yz}^{(1)}, Q_{zx}^{(1)}, Q_{xy}^{(1)}) = (\rho_z \tau_z + \rho_y \tau_y, \rho_z - \rho_z \tau_x, \tau_z - \rho_x \tau_z), \quad (31)$$

$$T_{2g}^+ : (Q_{yz}^{(2)}, Q_{zx}^{(2)}, Q_{xy}^{(2)}) = (\rho_z \tau_z - \rho_y \tau_y, \rho_z + \rho_z \tau_x, \tau_z + \rho_x \tau_z), \quad (32)$$

$$T_{1g}^- : (M_x, M_y, M_z) = (\rho_y \tau_z - \rho_z \tau_y, -\rho_y + \rho_y \tau_x, \tau_y - \rho_x \tau_y), \quad (33)$$

$$T_{2g}^- : (T_{yz}, T_{zx}, T_{xy}) = (\rho_y \tau_z + \rho_z \tau_y, \rho_y + \rho_y \tau_x, \tau_y + \rho_x \tau_y), \quad (34)$$

where ρ_α and τ_β are 2×2 Pauli matrices representing physical spaces spanned by A-B and C-D, and (AB)-(CD), respectively (see the main text).

Next, we take into account bond degrees of freedom by connecting upward and downward tetrahedra in the pyrochlore structure. As the multipole degrees of freedom in Eqs. (29)-(34) are even-parity, asymmetric bond modulations with respect to each atomic site are necessary for describing spontaneous parity-breaking orders. By focusing on the nearest-neighbor bond modulations (see the main text), we can introduce a mean-field Hamiltonian for spontaneous parity breaking in the following form:

$$\begin{aligned} \mathcal{H}^{\text{OP}}(\mathbf{k}) &= \begin{pmatrix} 0 & -i\delta_{\text{AB}} \sin\left(\frac{k_x}{4} + \frac{k_y}{4}\right) & -i\delta_{\text{AC}} \sin\left(\frac{k_x}{4} + \frac{k_z}{4}\right) & -i\delta_{\text{AD}} \sin\left(\frac{k_y}{4} + \frac{k_z}{4}\right) \\ i\delta_{\text{AB}}^* \sin\left(\frac{k_x}{4} + \frac{k_y}{4}\right) & 0 & i\delta_{\text{BC}} \sin\left(\frac{k_y}{4} - \frac{k_z}{4}\right) & i\delta_{\text{BD}} \sin\left(\frac{k_x}{4} - \frac{k_z}{4}\right) \\ i\delta_{\text{AC}}^* \sin\left(\frac{k_x}{4} + \frac{k_z}{4}\right) & -i\delta_{\text{BC}}^* \sin\left(\frac{k_y}{4} - \frac{k_z}{4}\right) & 0 & i\delta_{\text{CD}} \sin\left(\frac{k_x}{4} - \frac{k_y}{4}\right) \\ i\delta_{\text{AD}}^* \sin\left(\frac{k_y}{4} + \frac{k_z}{4}\right) & -i\delta_{\text{BD}}^* \sin\left(\frac{k_x}{4} - \frac{k_z}{4}\right) & -i\delta_{\text{CD}}^* \sin\left(\frac{k_x}{4} - \frac{k_y}{4}\right) & 0 \end{pmatrix} \quad (35) \\ &= \frac{1}{2}(\rho_y + \rho_y \tau_z) \text{Re}[\delta_{\text{AB}}] \sin\left(\frac{k_x}{4} + \frac{k_y}{4}\right) - \frac{1}{2}(\rho_y - \rho_y \tau_z) \text{Re}[\delta_{\text{CD}}] \sin\left(\frac{k_x}{4} - \frac{k_y}{4}\right) \\ &+ \frac{1}{2}(\tau_y + \rho_z \tau_y) \text{Re}[\delta_{\text{AC}}] \sin\left(\frac{k_x}{4} + \frac{k_z}{4}\right) - \frac{1}{2}(\tau_y - \rho_z \tau_y) \text{Re}[\delta_{\text{BD}}] \sin\left(\frac{k_x}{4} - \frac{k_z}{4}\right) \\ &+ \frac{1}{2}(\rho_x \tau_y + \rho_y \tau_x) \text{Re}[\delta_{\text{AD}}] \sin\left(\frac{k_y}{4} + \frac{k_z}{4}\right) - \frac{1}{2}(\rho_x \tau_y - \rho_y \tau_x) \text{Re}[\delta_{\text{BC}}] \sin\left(\frac{k_y}{4} - \frac{k_z}{4}\right) \\ &+ \frac{1}{2}(\rho_x + \rho_x \tau_z) \text{Im}[\delta_{\text{AB}}] \sin\left(\frac{k_x}{4} + \frac{k_y}{4}\right) - \frac{1}{2}(\rho_x - \rho_x \tau_z) \text{Im}[\delta_{\text{CD}}] \sin\left(\frac{k_x}{4} - \frac{k_y}{4}\right) \\ &+ \frac{1}{2}(\tau_x + \rho_z \tau_x) \text{Im}[\delta_{\text{AC}}] \sin\left(\frac{k_x}{4} + \frac{k_z}{4}\right) - \frac{1}{2}(\tau_x - \rho_z \tau_x) \text{Im}[\delta_{\text{BD}}] \sin\left(\frac{k_x}{4} - \frac{k_z}{4}\right) \\ &+ \frac{1}{2}(\rho_x \tau_x - \rho_y \tau_y) \text{Im}[\delta_{\text{AD}}] \sin\left(\frac{k_y}{4} + \frac{k_z}{4}\right) - \frac{1}{2}(\rho_x \tau_x + \rho_y \tau_y) \text{Im}[\delta_{\text{BC}}] \sin\left(\frac{k_y}{4} - \frac{k_z}{4}\right), \quad (36) \end{aligned}$$

where $\delta_{ij} = \text{Re}[\delta_{ij}] + i\text{Im}[\delta_{ij}]$ is the complex variable describing the bond modulation between sublattices i and j ($i, j = \text{A-D}$); the real and imaginary parts of δ_{ij} represent the bond modulations with time-reversal even and odd, respectively. $\mathcal{H}^{\text{OP}}(\mathbf{k})$ is a part of $[f_{\alpha\beta 0}^{\text{A}}(\mathbf{k})\rho_\alpha\tau_\beta]_{ij}^{\sigma\sigma}$ in Eq. (1) in the main text. By writing down the bond degrees of freedom as $\tilde{\delta} = (\delta_{\text{AB}}, \delta_{\text{AC}}, \delta_{\text{AD}}, \delta_{\text{BC}}, \delta_{\text{BD}}, \delta_{\text{CD}})$, the irreducible representations for the bond modulations are obtained as $\tilde{\delta}_{Q_{xyz}} = \delta(1, 1, 1, 1, 1, 1)$ belonging to A_{2u}^+ , $(\tilde{\delta}_{G_u}, \tilde{\delta}_{G_v}) = [\delta(2, -1, -1, -1, -1, 2), \delta(0, 1, -1, -1, 1, 0)]$ belonging to E_u^+ , and $(\tilde{\delta}_{Q_x}, \tilde{\delta}_{Q_y}, \tilde{\delta}_{Q_z}) = [\delta(0, 0, -1, 1, 0, 0), \delta(0, -1, 0, 0, 1, 0), \delta(-1, 0, 0, 0, 0, 1)]$ belonging to T_{1u}^+ with time-reversal even, while they are given by $(\tilde{\delta}_{T_x}, \tilde{\delta}_{T_y}, \tilde{\delta}_{T_z}) = [\delta(i, i, 0, 0, -i, -i), \delta(i, 0, i, -i, 0, i), \delta(0, i, i, i, i, 0)]$ belonging to T_{1u}^- and $(\tilde{\delta}_{M_{yz}}, \tilde{\delta}_{M_{zx}}, \tilde{\delta}_{M_{xy}}) = [\delta(-i, i, 0, 0, -i, i), \delta(i, 0, -i, i, 0, i), \delta(0, -i, i, i, -i, 0)]$ belonging to T_{2u}^- with time-reversal odd. By substituting these modulations into Eq. (36), the microscopic expressions for ETQs are obtained as Eqs. (2), (3), (8)-(13) in the main text. Note that these expressions can be rewritten in terms of the multipole degrees of freedom in Eqs. (29)-(34), which are

given by

$$G_u = \frac{1}{2} [c_x s_x (M_x - T_{yz}) + c_z s_y (M_y + T_{zx}) - s_z \{c_x (M_z + T_{xy}) + c_y (M_z - T_{xy})\}], \quad (37)$$

$$G_v = \frac{1}{2} [s_x \{2c_y (M_x + T_{yz}) + c_z (M_x - T_{yz})\} - s_y \{2c_x (M_y - T_{zx}) + c_z (M_y + T_{zx})\} - s_z \{c_x (M_z + T_{xy}) - c_y (M_z - T_{xy})\}], \quad (38)$$

$$T_x = \frac{1}{6} \left[3c_x \left\{ s_y (Q_{xy}^{(2)} - Q_{xy}^{(1)}) + s_z (Q_{zx}^{(2)} - Q_{zx}^{(1)}) \right\} + s_x \left\{ c_y (2Q_0^{(2)} + Q'_u + 3Q'_v) + c_z (2Q_0^{(2)} + Q'_u - 3Q'_v) \right\} \right], \quad (39)$$

$$T_y = \frac{1}{6} \left[3c_y \left\{ s_z (Q_{yz}^{(2)} - Q_{yz}^{(1)}) + s_x (Q_{xy}^{(2)} - Q_{xy}^{(1)}) \right\} + s_y \left\{ c_z (2Q_0^{(2)} + Q''_u + 3Q''_v) + c_x (2Q_0^{(2)} + Q''_u - 3Q''_v) \right\} \right], \quad (40)$$

$$T_z = \frac{1}{6} \left[3c_z \left\{ s_x (Q_{zx}^{(2)} - Q_{zx}^{(1)}) + s_y (Q_{yz}^{(2)} - Q_{yz}^{(1)}) \right\} + s_z \left\{ c_x (2Q_0^{(2)} + Q_u + 3Q_v) + c_y (2Q_0^{(2)} + Q_u - 3Q_v) \right\} \right], \quad (41)$$

$$M_{yz} = \frac{1}{6} \left[3c_x \left\{ -s_y (Q_{xy}^{(2)} - Q_{xy}^{(1)}) + s_z (Q_{zx}^{(2)} - Q_{zx}^{(1)}) \right\} - s_x \left\{ c_y (2Q_0^{(2)} + Q'_u + 3Q'_v) - c_z (2Q_0^{(2)} + Q'_u - 3Q'_v) \right\} \right], \quad (42)$$

$$M_{zx} = \frac{1}{6} \left[3c_y \left\{ -s_z (Q_{yz}^{(2)} - Q_{yz}^{(1)}) + s_x (Q_{xy}^{(2)} - Q_{xy}^{(1)}) \right\} - s_y \left\{ c_z (2Q_0^{(2)} + Q''_u + 3Q''_v) - c_x (2Q_0^{(2)} + Q''_u - 3Q''_v) \right\} \right], \quad (43)$$

$$M_{xy} = \frac{1}{6} \left[3c_z \left\{ -s_x (Q_{zx}^{(2)} - Q_{zx}^{(1)}) + s_y (Q_{yz}^{(2)} - Q_{yz}^{(1)}) \right\} - s_z \left\{ c_x (2Q_0^{(2)} + Q_u + 3Q_v) - c_y (2Q_0^{(2)} + Q_u - 3Q_v) \right\} \right], \quad (44)$$

where we define $2(Q'_u, Q'_v) = (-Q_u + 3Q_v, -Q_u - Q_v) \propto (3x^2 - r^2, y^2 - z^2)$ and $2(Q''_u, Q''_v) = (-Q_u - 3Q_v, Q_u - Q_v) \propto (3y^2 - r^2, z^2 - x^2)$ for notational simplicity.
